

Optimized Measurements of UAV Mass Moment of Inertia with a Bifilar Pendulum

Matt R. Jardin*

The MathWorks, Inc., Natick MA 01760

Eric R. Mueller†

NASA Ames Research Center, Moffett Field, CA 94035

A bifilar (two-wire) pendulum is a torsional pendulum consisting of a test object suspended by two thin parallel wires. The pendulum oscillates about the vertical axis. The restoring torque of the bifilar pendulum is provided by the gravitational force as rotations from the rest state cause the test object to raise slightly. The mass moment of inertia is computed using dynamic modeling, measurements of the oscillation period, and the physical dimensions of the bifilar pendulum such as the length and separation displacement of the pendulum wires. A simulation technique is described that improves estimates of the mass moment of inertia by considering the nonlinear effects of damping and large angular displacements. An analysis of the error variance of mass moment of inertia measurements is also described. The resulting expression for the error variance is used to optimize the physical parameters of the bifilar pendulum to obtain the moment of inertia measurement with the minimum error variance. Monte Carlo simulations were used to validate the parameter optimization technique. Experimental results are presented for a uniform-density test object for which the moment of inertia is straightforward to compute from geometric considerations. Results are also presented for a small unmanned air vehicle, which was the intended application for this moment of inertia measurement technique.

I. Introduction

Measurements or computational estimates of mass moment of inertia are needed during the design and construction of aircraft, including unmanned air vehicles (UAVs), which have received sustained interest in recent years. The bifilar (two-wire) pendulum is an apparatus that has been used for the measurement of aircraft mass moments of inertia since near the time of the invention of the airplane because of its simplicity, safety, and relatively high accuracy.¹ The bifilar pendulum, shown in Fig. 1, is a torsional pendulum that consists of a test object suspended by two thin parallel wires of length h and separation displacement D . The pendulum oscillates about its vertical axis. A tare platform is often used to help configure the test object and to provide a tare mechanism for improving measurement accuracy. The rotation angle in the horizontal plane is θ . The restoring torque of the bifilar pendulum is provided by the gravitational force as rotations from rest cause the test object to raise slightly. Dynamic modeling is used to relate the measurable parameters of average oscillation period, wire length and wire separation displacement to the moment of inertia of the test object.

In the early experimental work by the National Advisory Committee for Aeronautics (NACA) that measured mass moment of inertia of small manned aircraft with a bifilar pendulum, the common technique was to ignore damping and to linearize the equations of motion to model the bifilar pendulum as an harmonic undamped oscillator.^{1,2} The bifilar pendulum was used for the measurement of moment of inertia about the yaw axis. While some reasoning was used to set apparatus parameters, the choice of specific parameters was not made based on any rigorously derived criteria, and there was no reported effort made to determine quantitative measurement errors due to apparatus dimensions.

*Senior Engineering Consultant, Consulting Services Group, 3 Apple Hill Drive. Associate Fellow AIAA.

†Aerospace Engineer, Automation Concepts Research Branch, MS 210-10. Member AIAA.

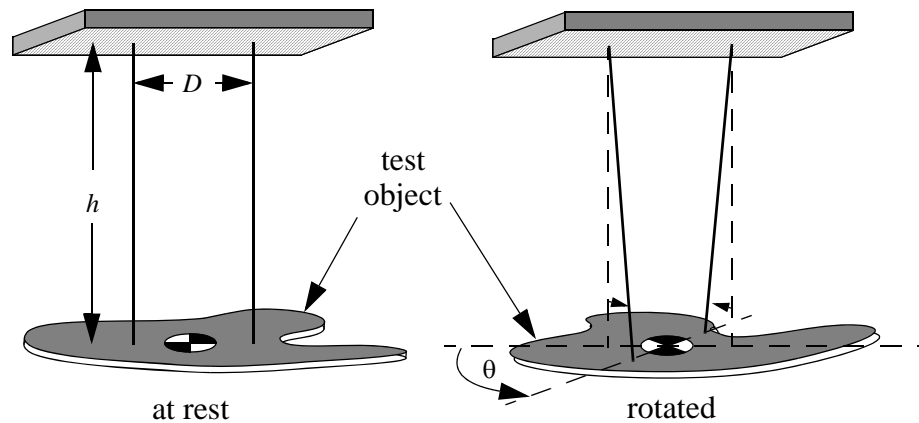


Figure 1. Bifilar pendulum diagrams

In later work, damping was still neglected, but researchers began to incorporate corrections to account for momentum transfer between the pendulum and the surrounding air.³ These corrections become important for test objects with large surface areas such as fixed wing aircraft, particularly when rotating about the roll axis. The motion of these objects entrains some of the air through which they rotate. The entrained air is most accurately modeled as an additional mass of the system rather than as a damping effect. This effect commonly appears in the literature on modeling and control of underwater manipulators where fluid momentum effects account for a significant portion of external forces on a body.¹⁰

A detailed nonlinear model of the bifilar pendulum was developed by Kane, primarily to examine the effects of uneven pendulum geometries.⁴ The nonlinear model was used to show that torsional motions of the bifilar pendulum are not significantly affected by uneven pendulum wire lengths or misaligned principal axes. Damping effects were not examined and the selection of apparatus dimensions was not discussed.

A report by de Jong⁵ provides an excellent background on the measurement of mass moments of inertia, particularly for aircraft. In de Jong's paper, a method for estimating multiple inertia parameters from a single experiment using statistical estimation techniques is described. Aerodynamic damping was accounted for in the development of the equations of motion, but not viscous damping. The equations of motion were then linearized to develop the estimation algorithms. Additional mass corrections were noted, but not addressed, as the main objective of the paper was to present a simplified procedure for measuring moment of inertia and not necessarily to improve the accuracy of the measurements.

The work by Lyons⁶ examined various hardware improvements and methodologies for improving modeling accuracy in a trifilar, or three-wire, pendulum. Errors due to linearization were mitigated by making accurate rig-tare measurements using objects with known moments of inertia. Precessional motions of the pendulum were an issue because only direct measurements of pendulum period for each oscillation were made with an optical sensor. Pendulum precession caused aliasing problems and variations in the measured rotational period. Damping effects were treated analytically, but not tested. The damping was modeled by a viscous (linear) damping term, but aerodynamic (square law) damping was not considered.

This paper builds on previous work by incorporating a higher-fidelity dynamic model of the bifilar pendulum, and by presenting a method for determining the pendulum physical parameters that will minimize measurement error variance. This is the first such optimization of bifilar pendulum parameters known to the authors. The nonlinear dynamics of the bifilar pendulum are derived, including the effects of large-angle oscillations, aerodynamic drag, and viscous damping on rotational motions. The moment of inertia is determined by varying parameters until the numerical solution to the nonlinear equations of motion matches observed data. Simulink⁷ Parameter Estimation is used to determine pendulum parameters which cause simulation output to match experimental data in a least square error sense.

For the purpose of optimizing pendulum dimensions and parameters, an approximate linearized equation of motion is derived for small angular displacements. The section on variance analysis shows how errors in measurements of pendulum parameters affect the accuracy of the measured moment of inertia. The variance analysis is used to show how the physical parameters of the pendulum may be chosen to minimize the error variance of moment of inertia estimates. The linearized solution also provides initial guesses of the moment of inertia for the nonlinear parameter estimations.

The results section of this paper presents details of moment of inertia experiments for an homogeneous aluminum bar with negligible damping and for the same aluminum bar with foam core damping paddles. Results are also presented for measurement of the moment of inertia of a small unmanned airplane about its yaw axis. The experimental apparatus and measurement methods are described, followed by presentation of the experimental results.

II. Dynamic Model of the Bifilar Pendulum

The dynamics of the bifilar pendulum are derived using a Lagrangian approach to eliminate the need to determine constraint forces which are not required for the determination of moments of inertia. A nonlinear model is derived, where aerodynamic drag effects and large angular displacements are considered.

A. Nonlinear Model

The general form of Lagrange's equation of motion is given by

$$\frac{d}{dt}\left(\frac{\partial L}{\partial \dot{\theta}}\right) - \frac{\partial L}{\partial \theta} = Q \quad (1)$$

where $L = T - V$ is the Lagrangian function, with T being the kinetic energy of the system and V being the potential energy of the system. Any nonconservative generalized force is captured by Q .

The total kinetic energy of the pendulum and test object is comprised of both rotational and translational components and is given by

$$T = \frac{1}{2}I\dot{\theta}^2 + \frac{1}{2}m\dot{z}^2 \quad (2)$$

where I is the moment of inertia about the vertical axis (the z -axis in Fig. 2), θ is the angular displacement about the vertical axis, m is the object mass, and z is the vertical displacement.

An expression for the vertical displacement in terms of the rotational displacement is derived from geometric considerations (Fig. 2) and is given by

$$z = h[1 - \sqrt{1 - (1/2)(D/h)^2(1 - \cos\theta)}] \quad (3)$$

The rate of change of z is then given by

$$\dot{z} = \frac{(h/4)(D/h)^2 \sin(\theta)}{\sqrt{1 - (1/2)(D/h)^2(1 - \cos\theta)}} \dot{\theta} \quad (4)$$

The ratio of translational kinetic energy to rotational kinetic energy, ρ_{KE} , is derived from Eqs. (2) and (4) and is given by

$$\rho_{KE} \equiv \frac{(1/2)m\dot{z}^2}{(1/2)mr_g^2\dot{\theta}^2} = \left(\frac{1}{16}\right)\left(\frac{h}{r_g}\right)^2\left(\frac{D}{h}\right)^4 \left[\frac{\sin^2\theta}{1 - \frac{1}{2}\left(\frac{D}{h}\right)^2(1 - \cos\theta)} \right] \quad (5)$$

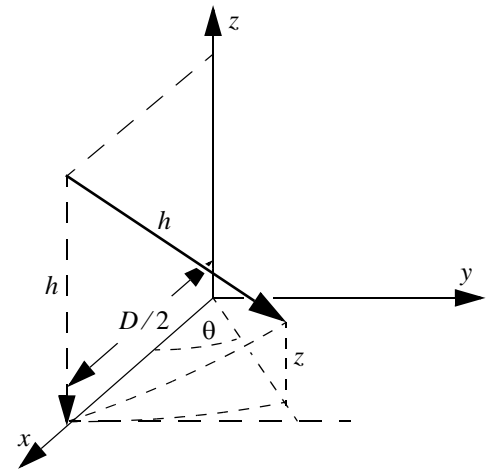


Figure 2. Geometry of the bifilar pendulum

where the moment of inertia, I , has been expressed in terms of mass, m , and radius of gyration, r_g . The term involving θ in Eq. (5) has a maximum value near unity at about $\theta = 90^\circ$ for h greater than D . For typical dimensions of the pendulum apparatus, the vertical translational kinetic energy of the system is small relative to the rotational energy and may safely be neglected. One may choose to continue the derivation using Eq. (2) for the kinetic energy, but the resulting equation of motion generally will not alter the results in a measurable way, nor does it change the linearized form of the equation of motion. One may use Eq. (5) to verify that translational kinetic energy is negligible for any particular experiment. If the pendulum apparatus is configured such that the ratio in Eq. (5) is not small, then one should include translational kinetic energy in the analysis. Translational kinetic energy has implicitly been neglected in past filar pendulum analyses.⁶

Assuming that the ratio in Eq. (5) is small, the kinetic energy of the bifilar pendulum is approximated as

$$T = \frac{1}{2}I\dot{\theta}^2 \quad (6)$$

The potential energy of the system is all due to vertical displacement, and is given by

$$V = mgz \quad (7)$$

The Lagrangian is then

$$L = \frac{1}{2}I\dot{\theta}^2 - mg(h - \sqrt{h^2 - 2(D/2)^2(1 - \cos\theta)}) \quad (8)$$

The damping associated with rotational motion of the pendulum is modeled by both aerodynamic drag and viscous damping. The damping is modeled by the following generalized force

$$Q = -K_D \cdot \dot{\theta} \cdot |\dot{\theta}| - C \cdot \dot{\theta} \quad (9)$$

where K_D and C are damping parameters that may be adjusted to match observed oscillation data.

Substituting into Eq. (1) and performing the derivative operations leads to the following nonlinear equation of motion for the bifilar pendulum

$$\ddot{\theta} + \left[\left(\frac{K_D}{I} \right) \dot{\theta} |\dot{\theta}| + \frac{C}{I} \dot{\theta} \right] + \left(\frac{mgD^2}{4Ih} \right) \frac{\sin\theta}{\sqrt{1 - (1/2)(D/h)^2(1 - \cos\theta)}} = 0 \quad (10)$$

B. Additional Mass Effects

For test objects with large surface areas that travel normal to the rotational direction, the dynamic system model must also include the momentum of air entrained by the test object during rotation.³ For a flat plate rotating such that it travels in a direction normal to the surface of the plate, aerodynamic theory gives the momentum of entrained air as

$$L_a = \left[\frac{k' \rho \pi c^2 b^3}{48} + \frac{k \rho \pi c^2 b l^2}{4} \right] \dot{\theta} \quad (11)$$

where L_a is the additional angular momentum of the system, k' is a coefficient of additional momentum, ρ is the air density, c is the chord length of the flat plate (which is normal to the air flow direction), b is the span of the flat plate, and k is a coefficient of additional mass. The two coefficients, k' and k , are functions of the aspect ratio and must be determined empirically for different test object configurations.

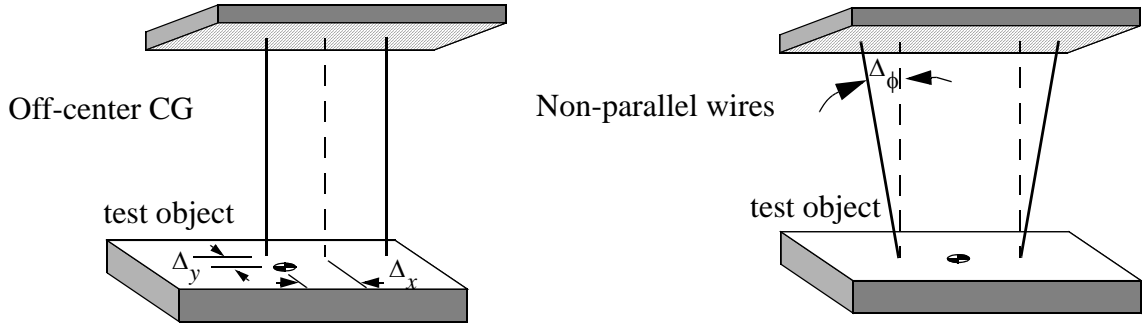


Figure 3. Unmodeled nonlinearities of the bifilar pendulum

The generalized force of the additional mass on the pendulum, Q_a , is found by taking the derivative of Eq. (11)

$$Q_a = \left[\frac{k' \rho \pi c^2 b^3}{48} + \frac{k \rho \pi c^2 b l^2}{4} \right] \ddot{\theta} = I_a \ddot{\theta} \quad (12)$$

When this additional force is incorporated in the equation of motion, the effect is the same as if the actual moment of inertia of the pendulum system was increased. The form of the equation of motion does not change, but the moment of inertia, I , in Eq. (10) must be understood to represent the total measured moment of inertia of the system, including additional mass effects. The moment of inertia of the test object is obtained from the total moment of inertia by subtracting the inertia due to additional mass

$$I_{to} = I - I_a \quad (13)$$

C. Unmodeled Phenomena

Several phenomena that may affect the accuracy of moment of inertia measurements have not been modeled in this work. By using a measurement platform or carriage and making tare measurements of the platform, one may mitigate the effects of unmodeled phenomena to some degree. Short descriptions of these unmodeled phenomena are now provided.

1. The effect of not centering the pendulum precisely around the center of mass has not been modeled (Fig. 3). A center of gravity (CG) displaced out of the plane formed by the two pendulum wires would cause the pendulum to shift until the CG was centered below the support points. This would result in an angular displacement, or tilting of the test object. An off-center CG along the line between the support wires would result in precessional motions in addition to the rotation about the z -axis. An attempt should be made to keep the CG centered when setting up the pendulum apparatus to mitigate any potential effects of a non-centered CG. In the case of the trifilar pendulum, additional motions would not be induced by an off-center CG, but a more complicated equation of motion would result, and additional measurements would be required to determine the moment of inertia from pendulum period measurements.⁶

2. The effect of non-parallel pendulum wires has not been modeled (Fig. 3). An attempt should be made to keep the wires as close to parallel as possible. Any angular displacement of the wires from the vertical will be small, since the height of the wires is typically greater than the displacement between the wires, and any error in wire attachment distance would be a small fraction of the displacement between the wires.

3. The effect of strain dynamics in the pendulum wires has not been considered. It is assumed that any additional strain displacement due to rotation will be small relative to the change in filament height, z , and that any displacement dynamics in the pendulum wires are much faster than those of the pendulum oscillations. This assumption has also been made in prior pendulum studies.⁶

4. The attachment of the wires at both the upper support and at the object being measured has been assumed to be moment-free. The wire itself may resist bending and twisting, or the type of wire attachment may offer some amount of bending and torsional resistance. The rotational displacement of the wires is small relative to the length of the wires, so bending and torsional resistance is assumed to be negligible.

5. The mass of the wires has not been accounted for. As the wires bend along with rotational displacement of the test mass, the CG of the wire also rises slightly. The mass of the wire is assumed to be small relative to the test mass such that this effect should be negligible. The unaccounted-for wire mass will also be mitigated by the rig tare measurements.

6. Rotation about a non-principal axis has not been modeled. Determining the principal axes of inertia for irregular nonhomogeneous objects can be challenging. For some common shapes, such as standard-configuration aircraft, a plane of symmetry helps determine one of the principal axes, but the alignment of the other two, which lie within the plane of symmetry, may still be difficult to determine. By examining the rotational equations of motion for a rigid body, one may readily see that if the body is not aligned along a principal axis, then various types of precession and wobble may be induced in the bifilar pendulum. The impact of these additional motions has been shown to not cause significant errors in the measurement of mass moment of inertia.⁴ If the off-diagonal terms of the inertia tensor are kept small, then the diagonal terms of the inertia tensor will remain dominant and can still be measured as described by the analysis in this paper. The error induced by assuming that a principal moment of inertia is being measured is related to $1 - \cos(\varepsilon)$, where ε is the angular displacement of the measurement axis from the principal axis. A one degree misalignment would result in a 0.015% error, while a ten degree misalignment would result in a 1.5% error.

III. Solving the Nonlinear Equation of Motion to Determine Mass Moment of Inertia

In prior work, experiments with filar pendulums were conducted while maintaining small angular displacements assuming that damping effects would not cause significant errors in the resulting estimates of the moment of inertia.^{1-3,5,6} The procedure was to measure the average oscillation frequency over many oscillations. The estimate of I was made from the solution to the linearized equation of motion. With computational tools now available for conveniently solving the nonlinear equation of motion via simulation, one may use numerical optimization techniques to determine values of the parameters that cause Eq. (10) to best fit experimental data. Solving the nonlinear equation of motion removes some of the restrictions that used to be placed on pendulum experiments when the moment of inertia was computed from the linearized equation of motion and produces more accurate results in a least-square error sense.

Simulink Parameter Estimation (SPE) is a suite of tools for pre-processing experimental data and numerically optimizing model parameters such that the difference between simulated model output and experimental data is minimized according to a user-chosen criteria (e.g., sum of squared errors or sum of absolute errors). The workflow for SPE is as follows:

1. Develop a dynamic model of the system under test. The inputs and outputs of the dynamic model must correspond to the inputs and outputs of the experiments to be run on the system.
2. Use SPE to import and pre-process the experimental data to prepare for parameter estimation. In the experimental runs for this paper, the first few raw data points were removed so that the experimental data would begin at rest ($\dot{\theta} = 0$). If required, the data preprocessing utility could also be used to filter or smooth the raw data using a variety of algorithms.
3. Choose the parameters and appropriate optimization options and run the parameter estimations.

A. Bifilar Pendulum Simulation Model

The bifilar pendulum model has been developed as a reusable library block in Simulink (Fig. 4). The inputs to the block are the parameters of the system under test: mass, m , moment of inertia, I , viscous damping coefficient, C , aerodynamic damping coefficient, K_D , and initial yaw angle, θ_0 . The output of the block is the measured yaw angle, θ . The block has been developed as a masked block so that the user may easily input different pendulum parameters via a mask dialog, such as the pendulum wire displacement, D , the wire height, h , and the uncertainty in the measurements of D , h , and measured yaw angle, θ . The pendulum model under the block mask has been developed directly from Eq. (10), with the only changes being the addition of code to introduce random errors into the pendulum parameters D and h , and angle measurement θ .

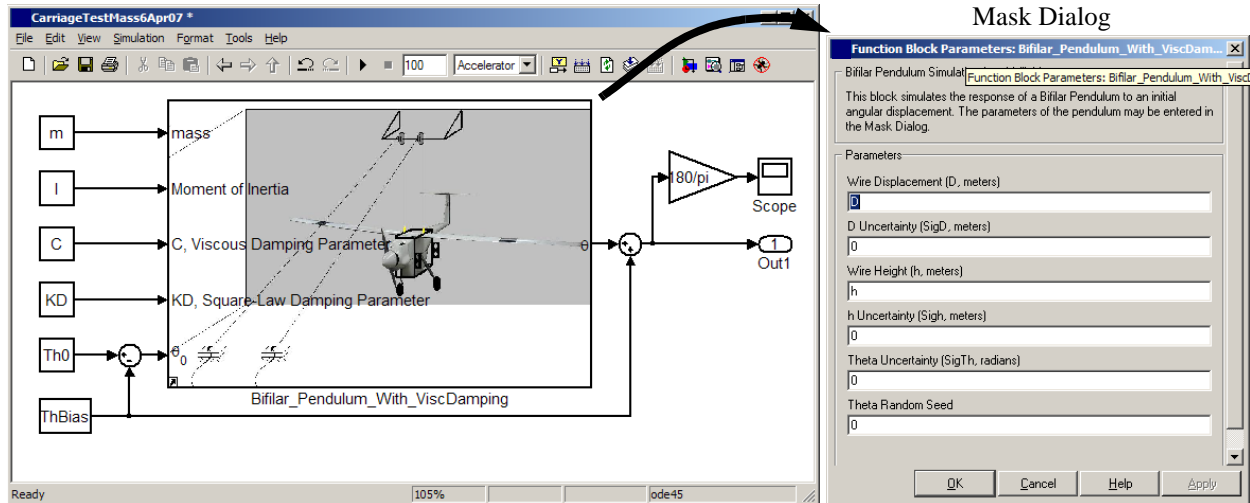


Figure 4. Model of the Bifilar Pendulum

B. Parameter Estimation Options

Once the simulation model has been developed and the experimental data have been imported and preprocessed, the parameter estimation options are selected. The first step is to choose which parameters will be estimated and to set the initial guess, the minimum and maximum values, and the typical values for each parameter. This information is used by SPE to scale the estimation problem for better numeric properties. The parameters to be estimated are the viscous damping coefficient, C , the mass moment of inertia, I , the aerodynamic damping coefficient, KD , the initial angular displacement, $Th0$, and the angular measurement bias, $ThBias$.

The next step is to set the simulation options and the optimization options within SPE. The simulation and parameter optimization options used for the estimations in this paper are provided in Fig. 5. In this paper, the nonlinear

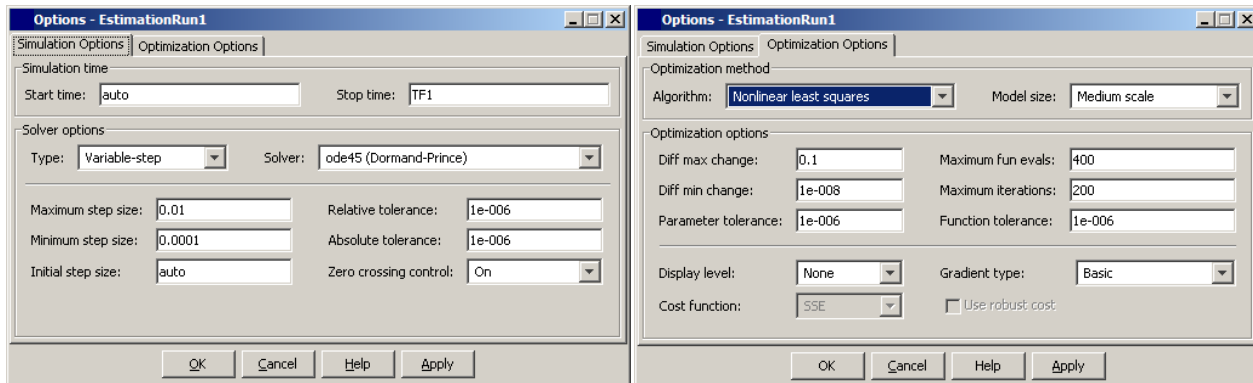


Figure 5. Simulation options for parameter estimation

least squares algorithm has been used, but other choices are gradient descent, pattern search, and simplex search. The cost function for the nonlinear least squares algorithm is the sum of the squared errors between measured and simulated data.

IV. Mass Moment of Inertia Error Variance Analysis

The choice of physical pendulum parameters such as D and h affects the accuracy of the measured mass moment of inertia. The goal of this section is to relate the error variance of the moment of inertia estimate directly to the error variance of empirical measurements. This analysis is then used to choose the parameters such that the variance of the mass moment of inertia error is minimized.

The approach is to express the moment of inertia as a function of the measured parameters. A small-perturbation analysis is performed to obtain an expression for the effects of perturbations in the measured parameters on the moment of inertia measurement. The resulting expression may be used to determine approximate optimum values for the physical pendulum parameters such that the variance in the moment of inertia estimate is minimized.

A. Linear Approximation

Using a describing function approximation⁸ of the aerodynamic damping term in Eq. (10) and using small-angle approximations leads to the following linear approximation of the equation of motion

$$\ddot{\theta} + \left[\left(\frac{K_D}{I} \right) \left(\frac{8A}{3\pi} \right) + \frac{C}{I} \right] \dot{\theta} + \left(\frac{mgD^2}{4Ih} \right) \theta = 0 \quad (14)$$

where A is an average oscillation amplitude, which may be selected to match the output of the nonlinear system and the approximate linear system.

The form of Eq. (14) represents a simple damped harmonic oscillator

$$\ddot{\theta} + 2\zeta\omega_n\dot{\theta} + \omega_n^2\theta = 0 \quad (15)$$

Comparing Eq. (14) and Eq. (15), one may solve for the mass moment of inertia in terms of the other measured parameters. This linear approximation to the pendulum equation of motion is now used to examine the effects of measurement error on resulting moment of inertia measurements.

B. Moment of Inertia Error Variance

An expression is now derived for the variance of the moment of inertia as a function of the error variance of each measurement that contributes to the moment of inertia calculation. The solution to the linearized equation of motion of the bifilar pendulum is used for this purpose.

Equating eqs. (14) and (15) and solving for I gives

$$I = \frac{mgD^2}{4h\omega_d^2}(1 - \zeta^2) \quad (16)$$

where the damped natural frequency is defined as

$$\omega_d \equiv \omega_n \sqrt{1 - \zeta^2} \quad (17)$$

Expanding this expression in a Taylor's Series leads to

$$\begin{aligned} \Delta I(m, D, h, \omega_d, \zeta) = & \frac{gD^2(1 - \zeta^2)}{4h\omega_d^2} \Delta m + \frac{mgD(1 - \zeta^2)}{2h\omega_d^2} \Delta D - \frac{mgD^2(1 - \zeta^2)}{4h^2\omega_d^2} \Delta h - \\ & \frac{mgD^2(1 - \zeta^2)}{2h\omega_d^3} \Delta \omega_d - \frac{mgD^2\zeta}{2h\omega_d^2} \Delta \zeta + (\text{higher order terms}) \end{aligned} \quad (18)$$

where all parameters in the coefficients of the perturbation variables are nominal or as-measured values. Substituting for the nominal value of I from Eq. (16) and dropping higher order terms leads to the following simpler form of Eq. (18)

$$\Delta I = \left(\frac{I}{m}\right)\Delta m + \left(\frac{2I}{D}\right)\Delta D - \left(\frac{I}{h}\right)\Delta h - \left(\frac{2I}{\omega_d}\right)\Delta\omega_d - \left(\frac{2I\zeta}{1-\zeta^2}\right)\Delta\zeta \quad (19)$$

Assuming that the errors in each of these measurements are uncorrelated, and dropping the damping perturbation term, because it is typically much smaller than the other terms, the variance in ΔI is given by

$$\sigma_I^2 = \left(\frac{I}{m}\right)^2 \sigma_m^2 + \left(\frac{2I}{D}\right)^2 \sigma_D^2 + \left(\frac{I}{h}\right)^2 \sigma_h^2 + \left(\frac{2I}{\omega_d}\right)^2 \sigma_{\omega_d}^2 \quad (20)$$

Each of the error variance terms on the right side of Eq. (20) are related to a direct measurement except for the ω_d term, which still must be written in terms of the basic measurements of length and time.

C. Damped Natural Frequency Error Variance

The error variance of the damped natural frequency is given by

$$\sigma_{\omega_d}^2 = \left(\frac{2\pi n}{t_n^2}\right)^2 \sigma_t^2 \quad (21)$$

where σ_t^2 is the error variance in the measurement of the time, t_n , of the n th oscillation. In terms of the measured damped natural frequency, Eq. (21) becomes

$$\sigma_{\omega_d}^2 = \left(\frac{\omega_d^2}{2\pi n}\right)^2 \sigma_t^2 \quad (22)$$

D. Supplemental Inertia Calculations

If more than one data run is made for a given configuration of the bifilar pendulum, the aggregate moment of inertia across all runs is computed as the simple mean, and the aggregate standard deviation of the measurements is computed as follows

$$\sigma_{\text{aggr}} = \frac{1}{n} \sqrt{\sum_i^n \sigma_i^2} \quad (23)$$

A carriage is used to hold test objects and to enable adjustment of the wire mounting and alignment of the pendulum apparatus. Since the carriage has non-negligible mass moment of inertia, its effects must be subtracted from the total inertia measurements to calculate the moment of inertia of the test object. Differences are simply computed as follows

$$I_b = I_{(a+b)} - I_a \quad (24)$$

and the corresponding standard deviations, assuming independent measurements, are given by

$$\sigma_{I_b} = \sqrt{\sigma_{I_{(a+b)}}^2 + \sigma_{I_a}^2} \quad (25)$$

Finally, if the test object has significant damping, one must make corrections for the effective additional mass of entrained air. The mass moment of inertia is measured according to the procedure outlined in this section, but the resulting value for I must be corrected using Eqs. (12) and (13).

V. Optimizing Pendulum Parameters for Minimum Inertia Error Variance

Within the physical constraints of the laboratory where the bifilar pendulum is to be constructed, one may choose from a wide range of heights and wire displacements for the apparatus. We now use the error variance expressions from the previous section to develop a method for selecting the physical parameters to minimize the resulting error in moment of inertia measurements.

A. Optimizing Pendulum Physical Parameters

Solving Eq. (16) for ω_d and substituting into Eq. (20) leads to the following expression for the variance in the measurement error of I

$$\sigma_I^2 = \left(\frac{I}{m}\right)^2 \sigma_m^2 + \left(\frac{2I}{D}\right)^2 \sigma_D^2 + \left(\frac{I}{h}\right)^2 \sigma_h^2 + \left(\frac{ImgD^2(1-\zeta^2)}{4h\pi^2 n^2}\right) \sigma_t^2 \quad (26)$$

This relationship may now be used to determine the best choices for the physical parameters of the bifilar pendulum. The parameters for which there is a choice are D , h , and n . The height of the pendulum, h , appears with an inverse relationship to the error variance. Increasing h decreases the relative error on the measurement of h , and a larger h also decreases the frequency of oscillation, which improves the accuracy of the period measurement. Larger values of h also reduce nonlinear effects so that the best choice of h is to make it as large as practical.

The number of oscillations, n , should also be made as large as practical. Since the initial rotation angle cannot be made very large and there is no control over the damping ratio, the best strategy is to allow as many oscillations as are easily discerned before small-scale nonlinear effects and disturbances become predominant as the oscillations damp out.

Finally, the displacement between the pendulum wires, D , must be chosen. This parameter appears both directly and inversely proportional to the inertia error variance, suggesting that an optimum value for D exists. Increasing the value of D decreases the relative error on the measurement of D , but increasing the value of D increases the frequency of oscillation, which reduces the relative accuracy of the time measurement.

Assuming all other parameters to be fixed, minimizing Eq. (26) with respect D , while holding other parameters fixed, leads to the following optimal value for the pendulum width

$$D_{\text{opt}} = 2 \left[(\pi n)^2 \left(\frac{\sigma_D}{\sigma_t} \right)^2 \frac{Ih}{mg(1-\zeta^2)} \right]^{1/4} \quad (27)$$

B. Validation of Parameter Optimality

An efficient and practical method for validating Eq. (27) is to run a series of Monte Carlo simulations of the nonlinear equations of motion with simulated errors with normal distributions on the pendulum parameters and on measurements of yaw angle and time. If actual experiments were used, other unmodeled effects would introduce additional errors in the measurement of moment of inertia error variance. The Monte Carlo simulation method allows us to focus on the specific relation, Eq. (27), that is being validated.

The Monte Carlo simulations are performed using the Simulink command-line application programming interface (API). Using the API, MATLAB⁷ scripts have been developed to run the model of the bifilar pendulum (Fig. 4) for a chosen test matrix. To solve for the mass moment of inertia for each simulation run, the SPE tool is again used. The SPE tool also has a command-line API so that it may be run in an automated batch mode.

The simulated test object is based on the uniform aluminum bar and support carriage that is evaluated experimentally later in this paper. The test object and pendulum parameter values for the Monte Carlo simulations are provided below in Tables 1-3. The simulation is run 50 times for each of the 5 values of D for a total of 250 simulation runs. The pendulum parameters are randomized once at the beginning of each simulation using the `randn()` function in MATLAB to generate normally distributed random errors with the standard deviations given in Table 3. The yaw

Table 1. Test Object Parameters		Table 2. Pendulum Parameters		Table 3. Modeled Parameter Uncertainty	
Parameter	Value	Parameter	Value(s)	Parameter	Value
I	0.6383 kg-m ²	D	{0.05; 0.2; 0.55; 1.0; 1.5}	σ_D	0.0016 m
m	7.8563 kg		m	σ_h	0.005 m
C	0.0046 kg-m ² /s		2.7353	σ_t	0.1 s
K_D	0.0069 kg-m ² /rad		m	σ_θ	0.0014 rad
θ_0	0.4463 rad	h		σ_m	0 kg
θ_{bias}	0 rad				

angle output is randomized at each time step, also according to the standard deviation in Table 3. Finally, to simulate time measurement errors, the final time of each simulation is randomized using `randn()`, and then the other time values of the simulation run are scaled accordingly. Each run takes about 0.2 seconds on average (on a ThinkPad T43, 2GHz, 1GB RAM), so the total time required for the simulations is less than one minute.

SPE is used to estimate the simulated test object parameters for each of the 250 Monte Carlo simulation runs, just as is done for real experimental data. The empirical standard deviation for each of the 5 sets of 50 runs is then computed. The results are plotted along with the theoretical curve of Eq. (26) for the pendulum and test object parameters given in Tables 1 through 3 (Fig. 6). The optimal value of pendulum wire width, D_{opt} , is also identified in Fig. 6. The simulation results match well with the theoretical curve and also indicate that the optimum value for D is predicted well by Eq. (27).

VI. Mass Moment of Inertia Experiments

The bifilar pendulum analysis techniques presented in this paper are now applied to the measurement of the moments of inertia of a small unmanned air vehicle (UAV). Before presenting results for the UAV, the moment of inertia of a test object (a thin aluminum bar) of known geometry, both with and without damping paddles, is measured to demonstrate the accuracy of the measurement apparatus. To simulate the high damping and additional mass effects of the UAV (especially about its roll axis), large flat pieces of foam core board are attached to the test object for one set of experimental runs. The moment of inertia of the aluminum bar is easily calculated from geometric measurements so that results of the pendulum experiments may be compared with truth data.

In this section, the pendulum apparatus and sensors are first described. This is followed by a discussion of the measurement procedure and data reduction techniques. The remaining subsections present results of measurement of the moment of inertia of the support carriage, the aluminum bar test object, the test object with damping paddles, and the UAV using the pendulum.

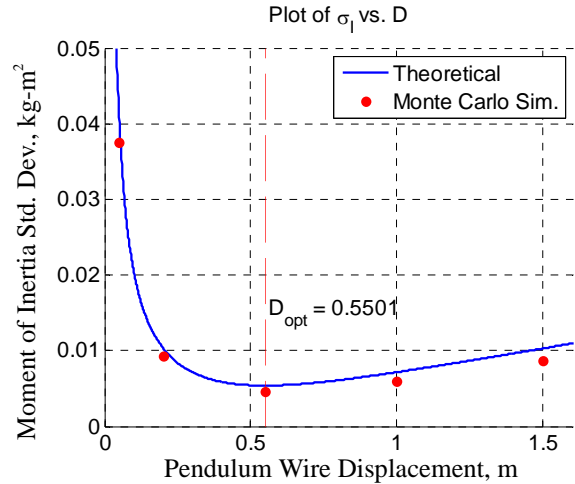


Figure 6. Monte Carlo simulation results.

A. Bifilar Pendulum Apparatus

The pendulum apparatus consisted of two steel wires that ran up from the carriage, over two pulleys, and down at an angle to the experiment floor below (Fig. 7). Each wire was attached to a short length of nylon rope that was subsequently anchored into a fairlead clam cleat, which allowed independent adjustment of the cable lengths. The pulleys were mounted between 2 m and 3 m above the floor, just high enough to hang the aircraft freely.

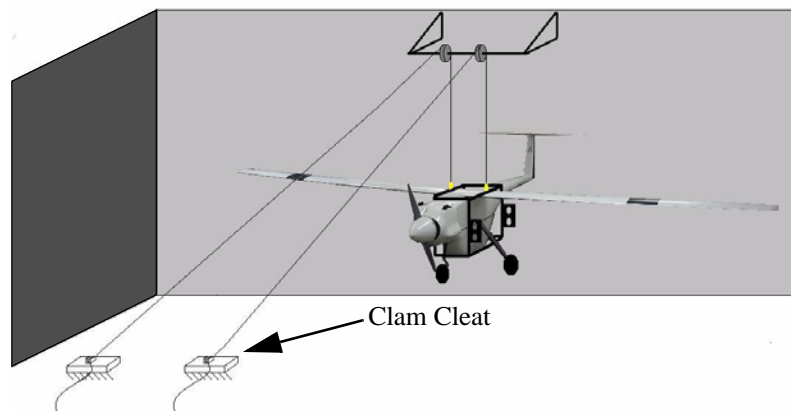


Figure 7. Bifilar Pendulum Apparatus

An aluminum carriage was used to support test objects. The carriage was custom-designed to mount to the UAV about any of its three principal axes (Fig. 8), and could also be used to support other test objects. The carriage contained three sets of mounting holes, one set for each axis. The mounting holes supported dual rotating slider rails, allowing the wires attached inside the rails to be connected to the carriage anywhere within a four inch radius of a mounting hole. This flexibility was required in order to adjust for the center of gravity position of the test object.

The experiments described in this section were performed in the recessed pit in hangar N210 at the NASA Ames Research Center.⁹ It is interesting to note that similar moment of inertia experiments had been performed in the same area of N210 more than a half a century ago before the conversion of the hangar for housing a six-degree-of-freedom motion flight simulator and office space. The deep pit is ideal for performing bifilar pendulum experiments because of its substantial depth and protection from air currents.

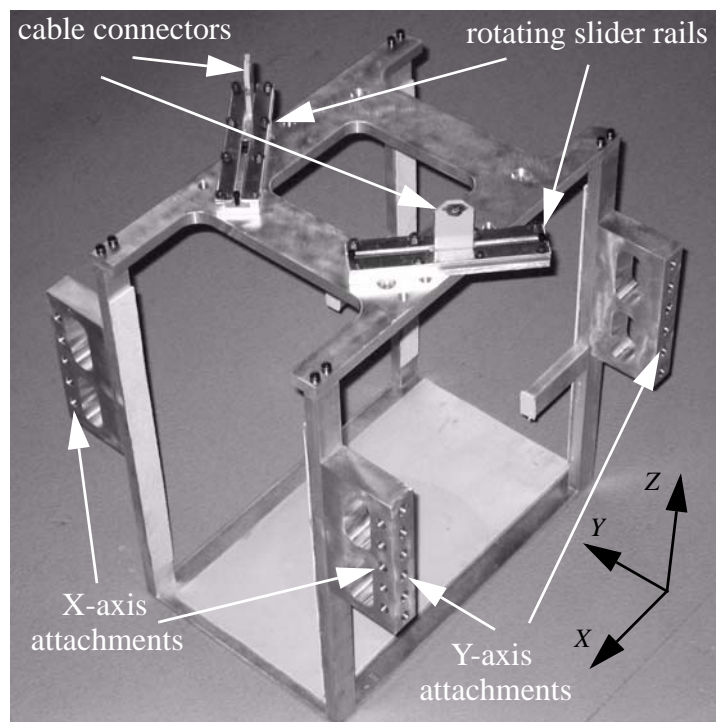


Figure 8. Bifilar Pendulum Support Carriage

B. Sensors and Measurements

The sensor for conducting moment of inertia measurement experiments was a small inertial navigation system called the MIDG-II, made by Microbotics.¹¹ The MIDG-II consists of three-axis rate gyros and accelerometers, a magnetometer, and a GPS receiver. The GPS was not used during the experiments, which were conducted indoors. Of the different modes of data output for the MIDG-II, the Vertical Gyro (VG) mode was employed during the experiments. In the VG mode, the angular displacement output of the MIDG-II is filtered along with accelerometer and magnetometer data to mitigate the effects of gyro drift. The attitude accuracy is reported by the manufacturer to be better than 0.4 degrees.

The MIDG-II horizontal plane was aligned with the pendulum apparatus using a bubble level to zero out the pitch and roll angles. The data acquisition software utility checked the alignment prior to each data run and stopped the experiment if pitch or roll misalignment was detected. Alignment of the yaw angle was not important since only heading differences from rest are required.

A custom software application was written to collect data from the MIDG-II. Audio cues were used to report the state of data collection since no visual displays were to be used during the experiments. The initialization procedure consisted of collecting data for one minute with the apparatus at-rest for checking pitch and roll alignment. If the alignment checked out, an audio signal was given so that oscillations could be initiated by the experiment operator. When the application detected a yaw displacement of greater than 30 degrees, data recording was started at a rate of 16.7 Hz, which was adequate for expected oscillation rates of less than 0.5 Hz. When the oscillation amplitude had decreased to less than one third of the initial amplitude, data acquisition was stopped and an audio cue was given.

C. Experimental Set-up

The pendulum apparatus, including carriage and test object, was hoisted so it hung just above the floor, and the wire lengths were adjusted at the clam cleats to be of equal length. The mounting rails on the carriage were then rotated, and the attachment points within the rails were adjusted until the wires were parallel and the principal axis of inertia was aligned with the pendulum wires. The distances between the wires and from the carriage to the pulleys were measured and recorded. Finally, the MIDG-II was mounted to a horizontal surface on the carriage and connected to the data acquisition computer. At this point, dimensions were recorded, and the experiment was initiated by turning on the data acquisition computer.

D. Data Reduction

A data logging and experiment check-list utility was developed to record physical parameters of the pendulum apparatus and other experiment details (Fig. 9). Simulink Parameter Estimation was used to determine the moment of inertia from experimental data as described in section III. Any necessary supplemental calculations were then made, such as accounting for the support carriage tare, or applying additional mass corrections. The experimental runs are now described.

E. Carriage Tare Measurements (Z-axis)

A tare measurement of the mass moment of inertia of the support carriage is made so that it can be subtracted from the moments of inertia of test objects made with the support carriage. The tare measurement also helps to reduce the effect of unmodeled system errors. In the case of the support carriage, the aerodynamic and viscous damping effects are very small. The additional mass effect is negligible due to the small surface area of the carriage, so this correction need not be applied.

The measured properties of the carriage and the pendulum apparatus are given in Table 4.

The mass moment of inertia of the support carriage has been measured using the parameter estimation technique described previously. A plot of the experimental results with the simulated results shows a close match between experimental and simulated pendulum response for both runs of the carriage tare measurement (Fig. 10). A plot of the residuals confirms that the fit is good (Fig. 11). The resulting estimated parameters from SPE for each run and the aggregate parameter values are listed in Table 5.

The screenshot shows a software utility window titled "Moment of Inertia Experiment Log: 161932_02Jun2005". It contains a NASA logo on the left and a blue icon with "VFO" on the right. The main area is divided into three sections:

- Experimenters:** Four text input fields labeled "Name: Experimenter #1" through "#4".
- Pre-Experiment Checklist:** A list of seven checkboxes:
 - ☐ Checked Apparatus Level?
 - ☐ Took Photograph of Apparatus?
 - ☐ Measured & Recorded D & h?
 - ☐ Measured & Recorded Cable Attachment Geometry?
 - ☐ Checked All Cable Attachments?
 - ☐ MIDG Securely Fastened and Aligned?
 - ☐ Measured Object CG relative to Carriage CG?
 - ☐ Will Remember to Record Approx. Start Time?
- Measures:**
 - A label "Approx. Start Time (after 5 beeps)" followed by a "HrMM" input field.
 - Input fields for "Upper Displacement (Du):" and "Lower Displacement (Dl):", each with "cm +/- mm" units.
 - Input fields for "height before exp (hb):" and "height after exp (ha):", each with "cm +/- mm" units.
 - A button labeled "Press Here to Write Data File:" followed by a "Generate File" button.
 - A button labeled "Press Here to Reset All Values:" followed by a "Reset" button.

Figure 9. Experiment Log Utility

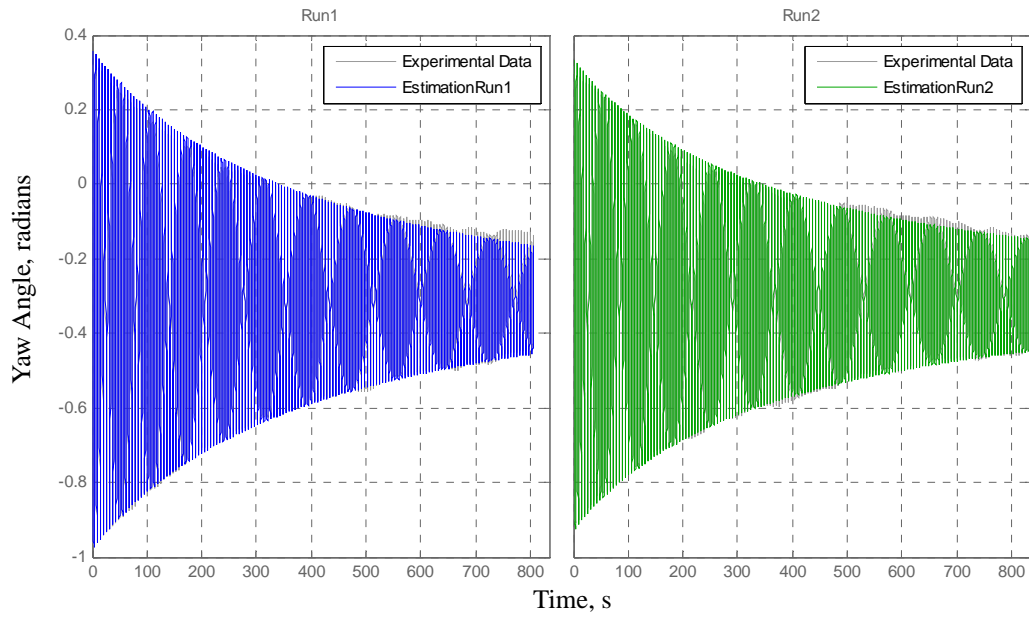


Figure 10. Plots of Experimental and Simulated Pendulum Response for Carriage Tare Measurement.

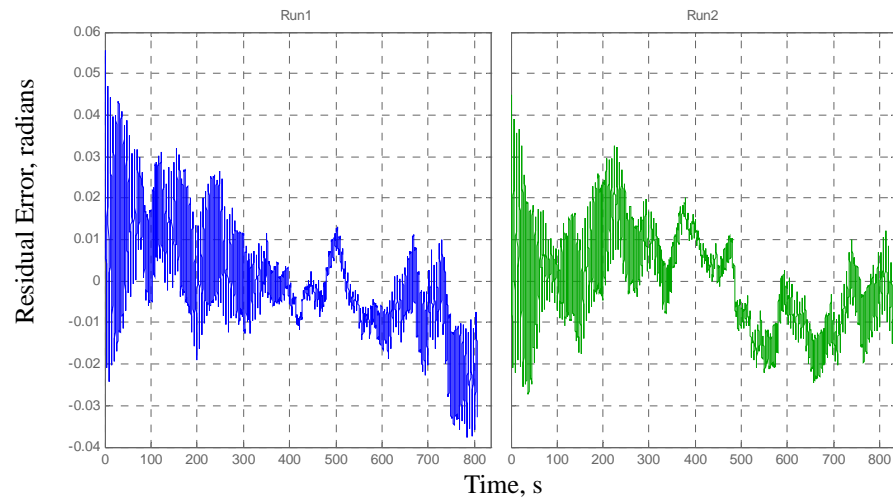


Figure 11. Residual Errors for both Carriage Tare Measurement Runs

Table 4. Carriage Tare: Pendulum and Test Object Properties

D (m)	h (m)	m (kg)	σ_D (m)	σ_h (m)	σ_m (kg)	σ_t (s)
0.2103	2.7321	6.31505	0.0016	0.0050	0.01	0.1

Table 5. Experimental Results for Carriage Tare

Run #	I (kg m ²)	σ_I (kg m ²)	K_D ((kg m ²)/rad)	C ((kg m ²)/s)	θ_0 (rad)	θ_{bias} (rad)
1	0.2050	0.0032	0.00076	0.00058	0.3479	-0.3103
2	0.2051	0.0032	0.00118	0.00044	0.3199	-0.2972
Aggregate	0.2050	0.0022	0.00097	0.00051	N/A	N/A

F. Mass Moment of Inertia of a Thin Aluminum Bar (Z-axis)

A set of experiments was run on an homogeneous thin aluminum bar of known geometry to compare pendulum measurements of moment of inertia with the value computed from geometric measurements and analysis. As with the carriage tare measurements, the damping terms are small, and the additional mass effect is again negligible.

The geometrically-computed moment of inertia of a homogeneous thin rectangular bar about the axis normal to the bar is given by

$$I_{\text{geom}} = \frac{1}{12}m(L^2 + T^2) \quad (28)$$

where m is the mass, L is the length, and T is the thickness of the bar. The following expression has been derived for the measurement error variance in the geometric moment of inertia

$$\sigma_{I_{\text{geom}}}^2 = \left(\frac{I}{m}\right)^2 \sigma_m^2 + \left(\frac{1}{6}mL\right)^2 \sigma_L^2 + \left(\frac{1}{6}mT\right)^2 \sigma_T^2 \quad (29)$$

where the values of the coefficients are computed with measured values. The measured geometric parameters and calculated mass moment of inertia are given in Table 6, and the measured properties of the pendulum apparatus are given in Table 7.

Table 6. Moment of Inertia and Geometric Properties of the Rectangular Aluminum Bar Test Object

I_{geom} (kg m ²)	$\sigma_{I_{\text{geom}}}$ (kg m ²)	Length L (m)	Width W (m)	Thickness T (m)	Mass m (kg)	σ_L (m)	σ_T (m)	σ_m (kg)
0.4306882	1.245×10^{-7}	1.8312	0.0381	0.007874	1.54122	7.5×10^{-4}	5×10^{-5}	1×10^{-5}

Table 7. Test Mass with Carriage: Pendulum and Test Object Properties

D (m)	h (m)	m (kg)	σ_D (m)	σ_h (m)	σ_m (kg)	σ_t (s)
0.2103	2.7353	7.85627	0.0016	0.0050	0.01	0.1

A plot of the SPE results along with the experimental data again shows that a good fit has been obtained (Fig. 12), and this is confirmed by the plot of residuals (Fig. 13). The estimated parameters from SPE for each run and the aggregate parameter values are given in Table 8.

Finally, the mass moment of inertia of just the test mass is computed by subtracting the carriage tare measurement, and the error standard deviation is computed using Eq. (25). These results are presented in (Table 9).

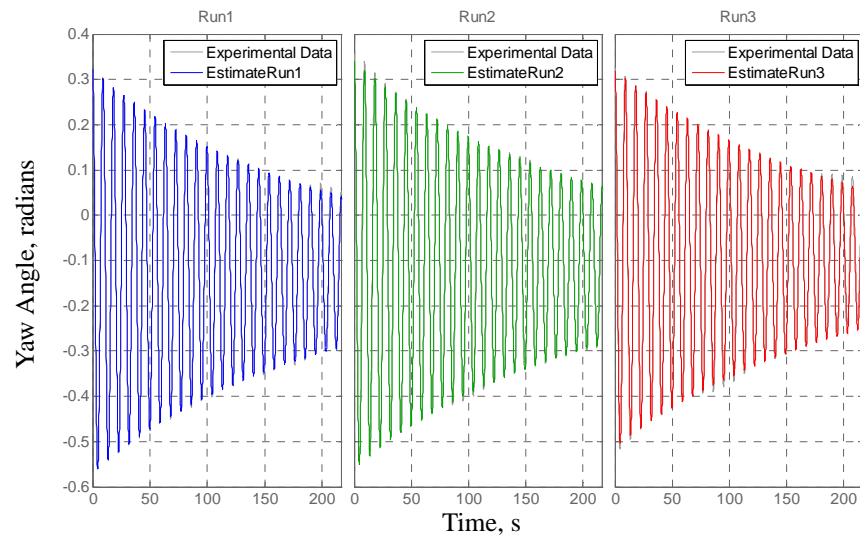


Figure 12. Plots of Experimental and Simulated Pendulum Response for Test Mass with Carriage.

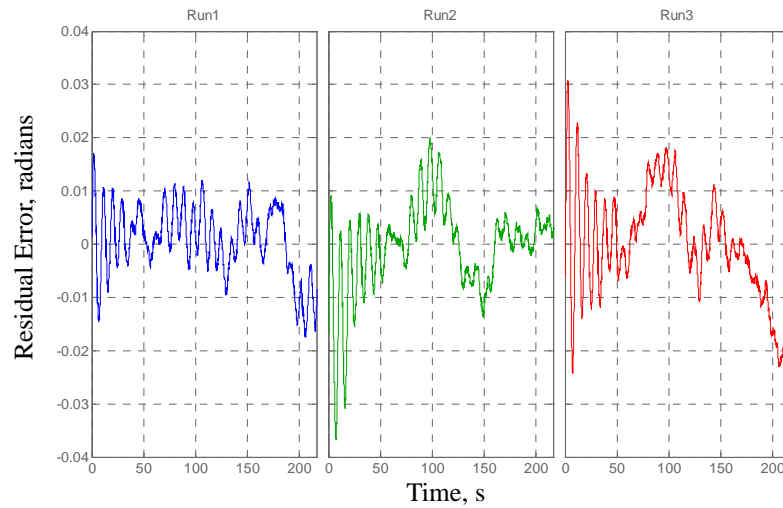


Figure 13. Residual Errors for Test Mass with Carriage

The moment of inertia of the test mass as measured by the pendulum experiments is well within the estimated error standard deviation.

Table 8. Experimental Results for Test Mass with Carriage

Run #	I (kg m ²)	σ_I (kg m ²)	K_D ((kg m ²)/rad)	C ((kg m ²)/s)	θ_0 (rad)	θ_{bias} (rad)
1	0.6383	0.0098	0.00692	0.00460	0.3219	-0.1244
2	0.6380	0.0098	0.00635	0.00448	0.3400	-0.1103
3	0.6379	0.0098	0.00120	0.00561	0.3195	-0.0963
Aggregate	0.6381	0.0057	0.00482	0.00490	N/A	N/A

Table 9. Measured and Calculated Mass Moment of Inertia of the Test Mass

Measurement Method	I	σ_I
Geometric	0.4306882	1.245×10^{-7}
Pendulum	0.4331	0.0061

G. Mass Moment of Inertia of a Thin Aluminum Bar with Damping Paddles (Z-axis)

To determine the accuracy of the bifilar pendulum for test objects with significant damping and additional mass effects, the test mass in the previous section was modified with two lightweight damping paddles made of thin, rigid foam core (Fig. 14). In this case, the additional mass effect must be considered when measuring the mass moment of inertia.

The moments of inertia of the damping paddles about their centers of mass are computed using Eq. (28). The geometry and computed mass moments of inertia of the two identical damping paddles are listed in Table 10. The moment of inertia of the damping paddles about the center of mass of the bar-paddle system, I_{pax} is computed using the parallel axis theorem

$$I_{\text{pax}} = I_{\text{paddle}} + m_{\text{paddle}} l^2 \quad (30)$$

and the corresponding variance is given by

$$\sigma_{I_{\text{pax}}}^2 = \sigma_{I_{\text{paddle}}}^2 + (l^4) \sigma_m^2 + (2m_{\text{paddle}} l)^2 \sigma_l^2 \quad (31)$$

where l is the distance from the center of mass of the system to the center of mass of the damping paddles. The geometrically computed moments of each of the paddles and the geometric mass moment of inertia of the bar-paddle system are given in Table 11. The total mass moment of inertia of the bar and 2-paddle system, I_{sys} , are given in Table 14.

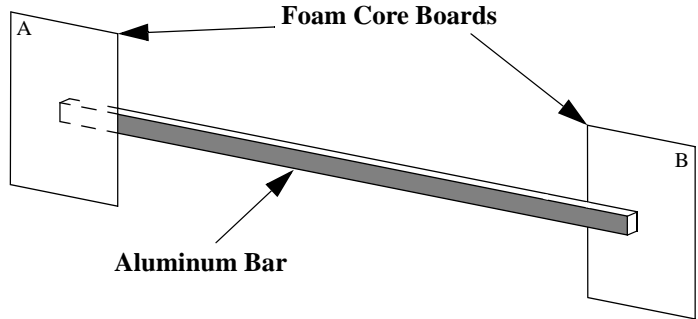
**Figure 14. Test Mass with Damping Paddles**

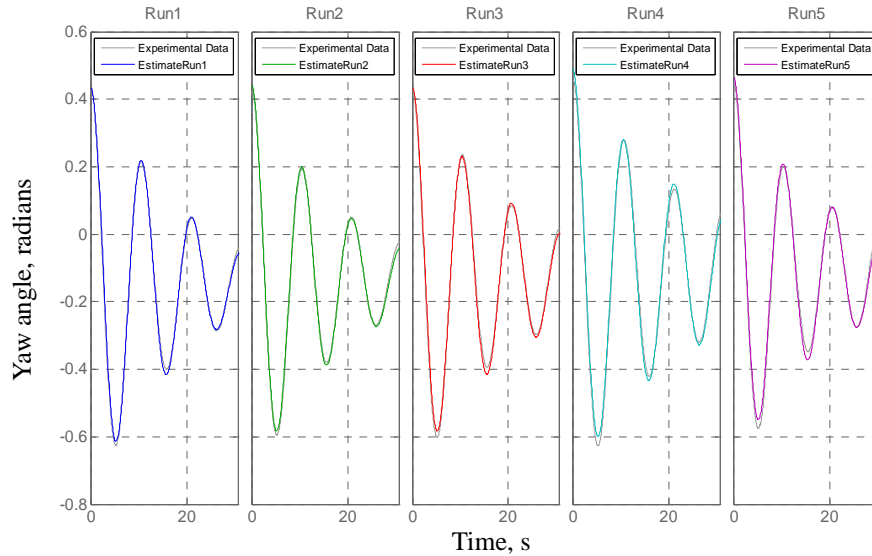
Table 10. Moment of Inertia and Geometric Properties of Each Foam Core Damping Paddle

I_{paddle} (kg m ²)	$\sigma_{I_{\text{paddle}}}$ (kg m ²)	Length L (m)	Width W (m)	Thickness T (m)	Mass m (kg)	σ_L (m)	σ_T (m)	σ_m (kg)
4.4292×10^{-4}	2.67×10^{-6}	0.254	0.508	0.00508	.08235	7.5×10^{-4}	1×10^{-5}	1×10^{-4}

Table 11. Computed mass moment of inertia of a single damping paddle about system center of mass

I_{pax} (kg m ²)	$\sigma_{I_{\text{pax}}}$ (kg m ²)	$I_{\text{paddle}} \text{ (A)}$ (kg m ²)	$I_{\text{paddle}} \text{ (B)}$ (kg m ²)	$\sigma_{I_{\text{paddle}}}$ (kg m ²)	l (m)	σ_l (m)
0.069478	1.4×10^{-4}	4.4292×10^{-4}	4.4292×10^{-4}	2.67×10^{-6}	0.9156	7.5×10^{-4}

The measured properties of the pendulum apparatus are given in Table 12. The plots of measured and simulated pendulum response (Fig. 15) and the corresponding residual plots (Fig. 16) for the 5 runs of this configuration again

**Figure 15. Plots of Pendulum Response for Test Mass with Damping Paddles and Carriage**

show close agreement between simulated and measured results. The pendulum experiment results are presented in Table 13. Subtracting the carriage tare measurement, The measured mass moment of inertia of the bar-paddle system after subtracting the carriage tare is given in Table 14 along with the geometrically-computed moment of inertia. The measured value is 12% higher than the value computed from geometric properties. For this configuration, additional mass corrections are required.

Table 12. Test Mass and Damping Paddles with Carriage: Pendulum and Test Object Properties

D (m)	h (m)	m (kg)	σ_D (m)	σ_h (m)	σ_m (kg)	σ_t (s)
0.2103	2.73685	8.021	0.0016	0.005	0.01	0.1

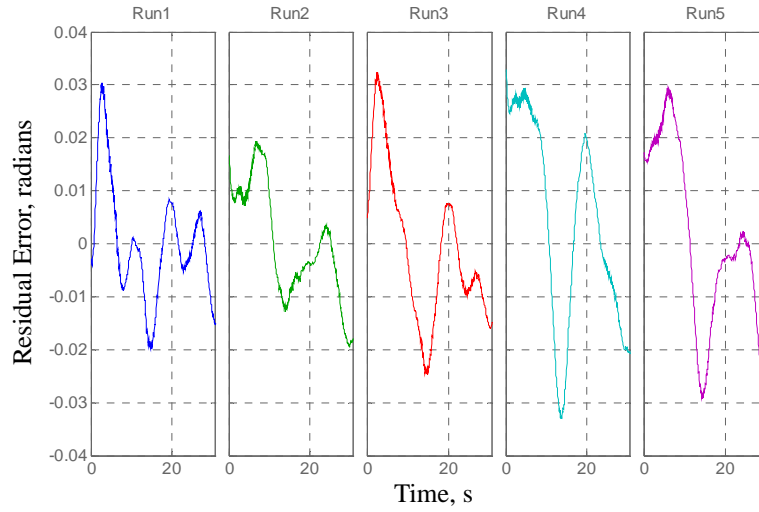


Figure 16. Residual Errors for Test Mass with Damping Paddles and Carriage

Table 13. Experimental Results for Test Mass and Damping Paddles with Carriage

Run #	I (kg m ²)	σ_I (kg m ²)	K_D ((kg m ²)/rad)	C ((kg m ²)/s)	θ_0 (rad)	θ_{bias} (rad)
1	0.8565	0.0143	-0.26455	0.13892	0.4350	-0.1449
2	0.8430	0.0141	-0.09982	0.11057	0.4424	-0.1376
3	0.8383	0.0140	-0.07735	0.08961	0.4328	-0.1306
4	0.8682	0.0145	0.02159	0.06400	0.4913	-0.1131
5	0.8246	0.0138	0.12246	0.06383	0.4659	-0.1185
Aggregate	0.8461	0.0063	-0.05953	0.09338	N/A	N/A

Table 14. Geometric mass moment of inertia of bar and 2-paddle system

measured I_{sys} (kg m ²)	geometric I_{sys} (kg m ²)	geometric $\sigma_{I_{\text{sys}}}$ (kg m ²)
0.6411	0.56965	2.8×10^{-4}

The parameters for computing additional mass corrections and the value of the coefficient of additional mass which was chosen to match observed data are given in Table 15. This empirically determined coefficient of additional mass corrects for the additional mass effect and causes the measured mass moment of inertia for the aluminum bar and damping paddle system to match with the geometrically calculated value.

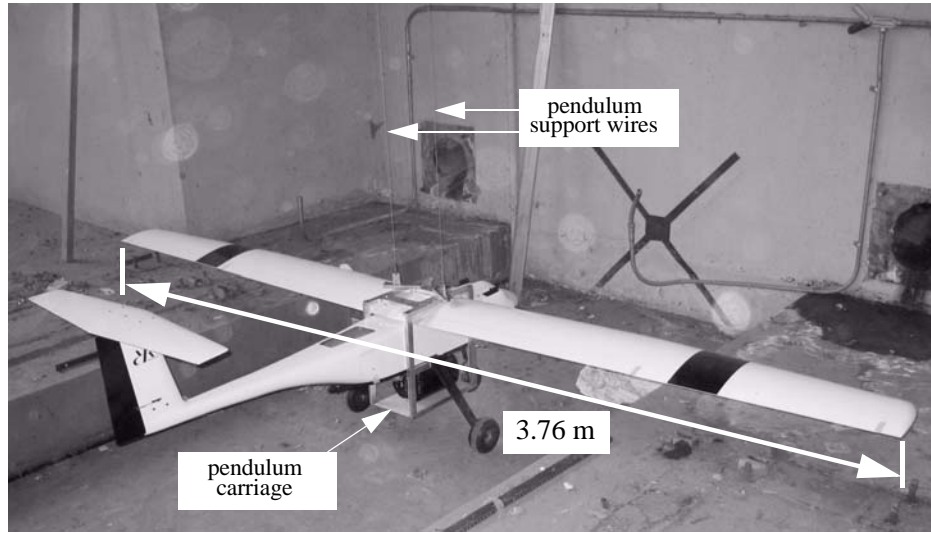
Table 15. Additional mass correction parameters

k (non-dimensional)	ρ_{air} (kg/m ³)	c (m)	b (m)	l (m)
0.673	1.23	0.508	0.254	0.9156

Correcting for large control surfaces on an airplane such as the vertical and horizontal stabilizers or the wing (when measuring roll moment of inertia) is a matter of approximating the surface areas exposed to the air during rotation. Some surfaces are well modeled as flat plates while others are irregular shapes. If extreme precision is required, one would need to develop more precise modeling techniques which are beyond the scope of this paper.

H. Mass Moment of Inertia of a Small UAV (Z-axis)

This final section is presented as a demonstration of the bifilar pendulum measurement technique for its intended application of measuring the mass moments of inertia of a small UAV (Fig. 17), the Flyer-Unmanned #1 (FU-1). The

**Figure 17. The FU-1 Aircraft and support carriage suspended for rotation about the yaw (Z) axis.**

measured properties of the carriage and the pendulum apparatus are given in Table 16. The results of the parameter estimation show relatively good agreement between simulated and experimental data (Fig. 18), although the residuals for the beginning part of the first experiment are a little higher than for the other experiments in this paper (Fig. 19). The resulting estimated parameters from SPE for each run and the aggregate parameter values are listed in Table 17.

Table 16. FU-1 Z-Axis: Pendulum and Test Object Properties

D (m)	h (m)	m (kg)	σ_D (m)	σ_h (m)	σ_m (kg)	σ_t (s)
0.2485	3.0375	24.11	0.001	0.006	0.0001	0.1

The additional mass corrections for the FU-1 now need to be made. Most of the large fuselage sections are near the pendulum rotation axis and are not expected to contribute much to the additional mass moment of inertia. The vertical stabilizer is a relatively large flat surface and is located far from the axis of rotation, so the additional mass effect of the vertical stabilizer will be accounted for.

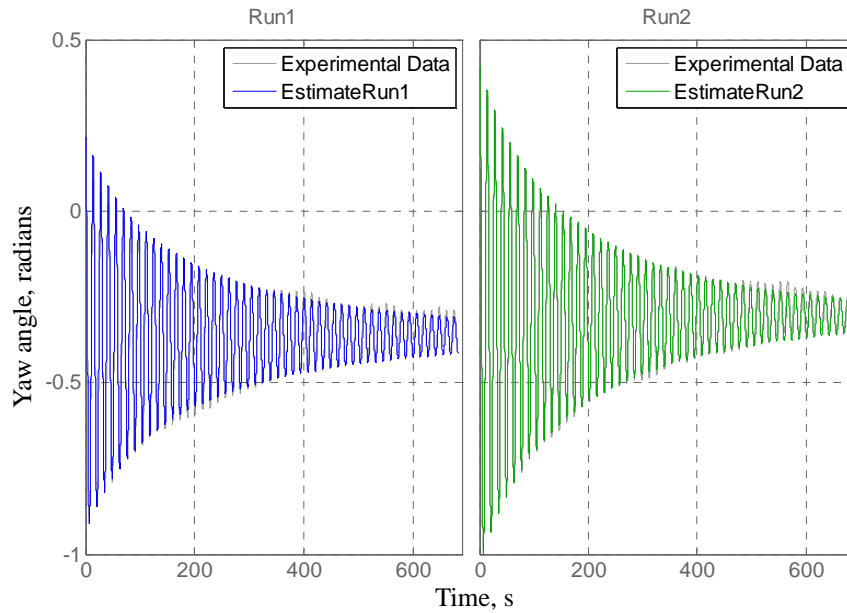


Figure 18. Experimental and Simulated Response for the FU-1 Aircraft (Z-axis) and Support Carriage.

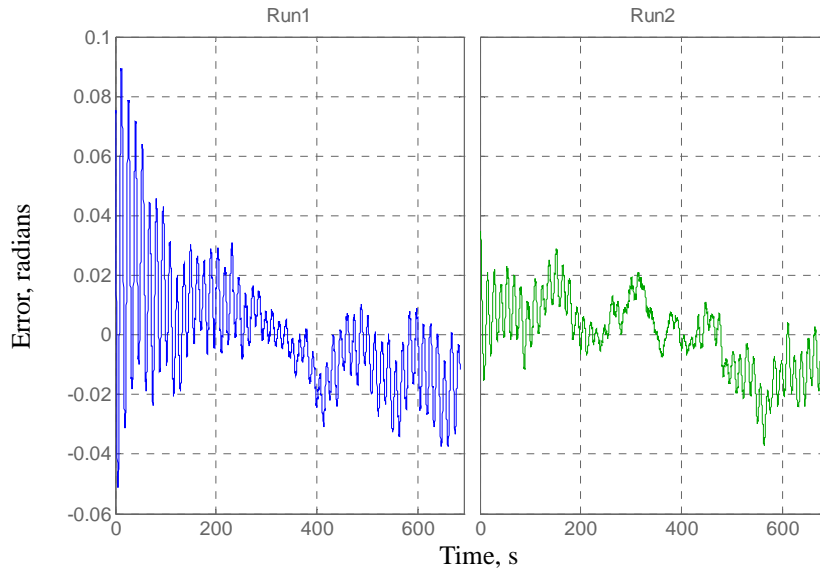


Figure 19. Residual Errors for FU-1 Aircraft (Z-Axis) with Support Carriage

The parameters for computing additional mass corrections of the vertical stabilizer, including the previously determined coefficient of additional mass, are provided in Table 18. In this case, the additional mass correction is roughly the same order of magnitude as the estimated error standard deviation in the measured moment of inertia.

Table 17. Experimental Results for FU-1 (Z-Axis) with Support Carriage

Run #	I (kg-m ²)	σ_I (kg-m ²)	K_D (kg-m ² /rad)	C (kg-m ² /s)	θ_0 (rad)	θ_{bias} (rad)
1	5.7691	0.0479	0.28790	0.02044	0.2156	-0.3628
2	5.7639	0.0479	0.18947	0.02990	0.4242	-0.3061
Aggregate	5.7665	0.0339	0.23869	0.02517	N/A	N/A

Table 18. Additional mass correction parameters: FU-1 vertical stabilizer

I_a (kg-m ²)	k (non-dimensional)	ρ_{air} (kg/m ³)	c (m)	b (m)	l (m)
0.0137	0.673	1.23	0.2159	0.3048	1.2192

VII. Conclusion

A method for measuring the mass moment of inertia of test objects with a bifilar pendulum is described in this report. The method is based on modeling the nonlinear equations of motion of the bifilar pendulum, including both aerodynamic and viscous damping forces. A nonlinear least squares parameter optimization algorithm is used to determine the parameters such that simulated data match experimental data. A discussion of the additional mass effect due to air entrainment was also provided.

An error variance analysis was presented to show how the moment of inertia measurement error is determined from basic experimental measurements of the pendulum apparatus parameters. A method for optimizing the physical parameters of the pendulum was also described such that the total measurement error of the moment of inertia is minimized. A Monte Carlo simulation technique was used to validate the derived expression for the error standard deviation of mass moment of inertia.

Experimental results were presented for the measurement of the moment of inertia of an homogeneous aluminum bar for which the moment of inertia could be accurately calculated based on geometric measurements alone. The pendulum measurements were within 0.5% of the geometrically determined moment of inertia, which is well within the estimated error standard deviation. Results were also presented for the same test object with large foam core damping paddles attached. The pendulum measurements for this case were about 12% higher than the geometrically determined moment of inertia, demonstrating the need for additional mass corrections. An empirical coefficient of additional mass was computed in order to match experimental results with the geometrically computed moment of inertia.

Experimental results have also been presented for the intended application of the inertia measurement techniques: the measurement of moment of inertia about the yaw axis of a small fixed wing UAV. These results demonstrate how the bifilar pendulum is used to measure mass moment of inertia in a practical setting, including how to compute the moment of inertia from raw experimental data, and how to apply additional mass corrections.

Acknowledgments

The authors wish to thank Dr. Tom Edwards, Dr. Jeff Schroeder, Dr. Banavar Sridhar, and Harry Swenson of Code AF at NASA Ames for their support of this work and their thoughtful reviews of this document. Dan Gundo helped to design and build the support carriage used in the UAV experiments and his efforts are much appreciated. The authors would also like to thank Dr. Fritz Moore for his assistance with accurate weighing of the components of the pendulum apparatus and the UAV. Finally, the authors would like to thank Dr. Ender St. John-Olcayto and Paul Smith of The MathWorks for their support of this work.

References

- ¹ Green, M. W., "Measurement of the Moments of Inertia of Full Scale Airplanes," NACA TN-265, 1927.
- ² Miller, M. P., "An Accurate Method of Measuring the Moments of Inertia of Airplanes," NACA TN-351, 1930.
- ³ Soulé, H. A., and Miller, M. P., "The Experimental Determination of the Moments of Inertia of Airplanes," NACA Rept. 467, 1933.
- ⁴ Kane, T. R., and Tseng, G.-T., "Dynamics of the Bifilar Pendulum," *International Journal of Mechanical Sciences*, Vol 9, Feb. 1967, pp. 83-96.
- ⁵ de Jong, R. C., and Mulder, J. A., "Accurate Estimation of Aircraft Inertia Characteristics from a Single Suspension Experiment," *Journal of Aircraft*, Vol. 24, No. 6, June 1987, pp. 362-370.
- ⁶ Lyons, D., "Obtaining Optimal Results with Filar Pendulums for Moment of Inertia Measurements," Paper No. 3237, *Weight Engineering*, Society of Allied Weight Engineers, Vol. 62, Issue #2, Winter 2002, pp. 5-20.
- ⁷ MATLAB[®] and Simulink[®], Software Package, Ver. R2007a, The MathWorks, Natick, MA, 2007.
- ⁸ Gelb, A., Vander Velde, W. E., "Multiple-Input Describing Functions and Nonlinear System Design," McGraw Hill, 1968.
- ⁹ Turner, H. L., "Measurement of the Moments of Inertia of an Airplane by a Simplified Method," NACA TN-2201, 1950.
- ¹⁰ McLain, T. W., Rock, S. M., "Development and Experimental Validation of an Underwater Manipulator Hydrodynamic Model," *International Journal of Robotics Research*, Vol 17, No. 7, July 1998, pp. 748-759.
- ¹¹ Microbotics, Inc. 28 Research Drive, Suite G, Hampton, VA 23666-1364.